ELSEVIER

Journal of Fluids and Structures 25 (2009) 1158–1176

JOURNAL OF FLUIDS AND STRUCTURES

www.elsevier.com/locate/jfs

Stochastic aerodynamics and aeroelasticity of a flat plate *via* generalised Polynomial Chaos

L. Bruno[a,*], C. Canuto[b], D. Fransos[b]

[a]*Politecnico di Torino, Department of Structural Engineering and Geotechnics, Viale Mattioli 39, I-10125 Torino, Italy*
[b]*Politecnico di Torino, Department of Mathematics, C.so Duca degli Abruzzi 24, I-10129 Torino, Italy*

Received 25 July 2008; accepted 15 June 2009
Available online 19 August 2009

Abstract

This paper deals with the characterisation of the aerodynamic and aeroelastic behaviour of a flat plate under uncertain flow conditions. The incoming mean flow velocity is described in terms of its probabilistic distribution, and the Reynolds number is consequently treated as a random variable. The objective of the study is to give a probabilistic description of the quantities which characterise the aerodynamics and aeroelasticity of a flat plate, i.e., steady forces, friction coefficient and velocity in the wake for the first and flutter derivatives for the second. Classical techniques such as Monte Carlo and quasi-Monte Carlo methods seem to be too expensive, in that they require many costly wind tunnel tests or numerical simulations of the steady and unsteady flow field around the motionless and moving plate. An efficient Multi-Element generalised Polynomial Chaos approach allows a significant reduction of the required number of realisations, making its cost affordable for real-world applications. The proposed method gives sufficiently accurate approximations of the probabilistic distributions of the desired quantities. Several examples of different representations of the stochastic outputs are given.

Keywords: Computational Wind Engineering; Flutter derivatives; Reynolds number effects; Uncertainty quantification; Generalised Polynomial Chaos

1. Introduction

Streamlined and bluff body aerodynamics and aeroelasticity are usually studied through experiments, mathematical models or a combination of the two, in which the parameters that define the models and the experimental set-up are considered to be known. This knowledge may come from other experiments or from theoretical considerations, but it is in general assumed as deterministic. Both aerodynamic and aeroelastic behaviour can be deeply affected by small variations of some of these parameters. Nevertheless, model or set-up parameters usually vary randomly, so that the aerodynamic and aeroelastic behaviour of a structure should be in general assumed as stochastic.

The mathematical methods which aim at the rigourous estimation of stochastic behaviour go under the name of *uncertainty quantification* methods. All of these methods require the uncertain parameters to be modelled through the introduction of *input* random variables that define the so-called *stochastic problem*. The law or some statistics of these

*Corresponding author. Tel.: +39 011 090 4870; fax: +39 011 090 4999.
E-mail address: luca.bruno@polito.it (L. Bruno).

0889-9746/$ - see front matter © 2009 Elsevier Ltd. All rights reserved.
doi:10.1016/j.jfluidstructs.2009.06.001

random variables must be known, in order to recover analogous information about the quantities that describe the aerodynamic and aeroelastic behaviour. Clearly, these quantities will be random variables themselves, and will be called *output* random variables. The most intuitive methods in the family of uncertainty quantification are the classical Monte Carlo (MC) and quasi-Monte Carlo methods (Caflisch, 1998), which make use of quasi-random number generation or properly defined point sets in order to explore the whole parameter space of the problem. A solution of the corresponding deterministic problem is associated with each realisation of the input random variables. A statistical analysis of these solutions provides the solution to the stochastic problem. The number of required realisations, however, may be prohibitively large. When the interest is in obtaining certain statistical quantities of the solution, such as the mean value, variance, kurtosis, or probability level sets, other techniques can be exploited, such as perturbation methods or Neumann-series expansion methods [see, e.g., Kleiber and Hien (1992), Deb et al. (2001), Schwab and Todor (2003)]. A more general approach is based on the global expansion of the random variables which define the stochastic problem into a basis of "elementary" random variables and the corresponding representation of the solution in terms of such variables. The most popular examples of such expansions are the Karhunen–Loève expansions [see, e.g., Loève (1977)], which involve the eigenfunctions of the covariance kernel of the random input, and the generalised Polynomial Chaos (gPC) expansions (Wiener, 1938; Ghanem and Spanos, 1991; Xiu and Karniadakis, 2002), which exploit the classical technology of weighted orthogonal polynomials. This approach allows the stochastic problem to be transformed into a corresponding deterministic problem in higher dimension. In the latter, the images of the basis random variables represent the new independent variables. The domain for these new variables is a tensor product of intervals of the real line. The high dimension of the new deterministic problem makes it necessary to re-examine and suitably tune classical solution techniques. The most common approaches to discretisation in the new variables rely on Galerkin projection methods (Xiu and Karniadakis, 2003), which can be used together with numerical integration techniques (Canuto and Kozubek, 2007), and on collocation methods (Babuška et al., 2007; Mathelin et al., 2005; Canuto and Fransos, 2009), which offer the opportunity of solving a number of corresponding deterministic realisations, as in MC methods, using a deterministic solver as a *black-box*.

In his review paper about uncertainty quantification in aeroelasticity, Pettit (2004) has pointed out that small uncertainties in the system parameters can significantly affect the aeroelastic system response. The main sources of uncertainties in aeroelastic systems include randomness in material properties, structural dimensions, structural boundary conditions and external excitations Beloiu et al. (2005), including incoming flow features. During the last decade, the methods described above have been adopted in the flutter analysis to include the quantification of the effects of system parametric uncertainty. For instance, MC methods have been used by Lindsley et al. (2006) to study the periodic response of nonlinear plate equations under supersonic flow subject to uncertain modulus of elasticity and structural boundary conditions, and by Poirel and Price (2003) to study the bending-torsion flutter under turbulent flow conditions with a linear structural model. Recent applications of the Polynomial Chaos expansion methods to flutter analysis are reviewed in Sarkar et al. (2009). In the same paper, the effect of parametric uncertainty on the stall flutter behaviour of a pitching airfoil is studied by applying both the Galerkin projection method and the collocation one: the plate-like structure is modelled as a 2-D rigid airfoil with torsional degree-of-freedom and the stall aerodynamic moment is computed using a semi-empirical dynamic stall model. Three structural parameters are assumed to be uncertain, their effect on the stall flutter system response being outlined in an earlier deterministic study by Sarkar and Bijl (2008).

The collocation method in the framework of the gPC approach is followed in this paper to quantify the effects of an uncertain incoming mean flow velocity. This quantity is modelled as a Weibull random variable, based on on-site experimental measurements, so that a random Reynolds number results. The effects of such an input random variable are investigated for both the aerodynamics and the aeroelasticity of the classical flat plate. As regards the aerodynamic behaviour, the dependence of the plate performance on the flow Reynolds number is well known. Several studies, e.g., Sun and Boyd (2004), highlighted the compressibility effects that arise at $\mathrm{Re}<10$ and that the main aerodynamic properties show high variations in the $10<\mathrm{Re}<10^3$ range. In the $10^3<\mathrm{Re}<\mathrm{Re}_{cr}$ range, the variations in the boundary layer shape and in the velocity profile in the wake are described by the classical Blasius and Goldstein analytical solutions respectively (Schlichting, 1979). Finally, for higher Re than the critical $\mathrm{Re}_{cr}\approx 5\times 10^5$ value, transition to turbulence occurs in the boundary layer. Flat plate aeroelasticity is also affected by Re variations: one of the first attempts to deterministically evaluate the Reynolds number effects on the flutter derivatives of a symmetrical airfoil was made by Halfman (1952) and then more recently by Le Maître et al. (2003). Reynolds number effects for such a streamlined body were the object of several deterministic investigations in a previous work by Bruno and Fransos (2008). A flat plate with an aspect ratio $B/D=400$ is considered in the present paper, along with a Reynolds number which varies through the whole $[0,+\infty)$ range. The specific uncertainty quantification method employed in the paper is described in Section 2, while the technology employed for the solution of the single deterministic realisations, which was introduced in a previous work (Fransos and Bruno, 2006), is briefly recalled in Section 3. The stochastic

characterisation of the steady flow around the motionless plate represents the first analysis step and is given in Section 4. Finally, the unsteady flowaround the moving plate and the resulting flutter derivatives are described in terms of random variables in Section 5. The efficiency of the proposed method is discussed in terms of reduced computational costs.

2. Mathematical methods of uncertainty quantification

Quantifying the uncertainty in some outputs of a system, due to the presence of uncertainty in the inputs and/or in the parameters which characterise the system itself, implies describing both the inputs and the outputs as random variables. The whole procedure proposed to obtain the approximate forms of the output moments and PDF is summarised in the flowchart in Fig. 1. Each block is detailed in the following.

Let us introduce a complete probability space $(\Omega, \mathscr{F}, \mathscr{P})$, where Ω is the outcome space, $\mathscr{F}$ is the set of events and $\mathscr{P}$ is a probability measure. When uncertainty is present, i.e., the inputs and parameters of a system depend on the outcome ω in the outcome space Ω, the classical representation of a deterministic dynamic system (Fig. 2(a)) must be modified in order to include this dependence (block 1, Fig. 2(b)). A single deterministic system corresponds to each single fixed outcome ω, i.e., to each *realisation*.

Let us introduce a generic *output random variable* η, for instance the output variable $o(t,\omega)$, e.g., the drag coefficient, of a stochastic aerodynamic system, or the transfer function $h(t,\omega)$ of a stochastic aeroelastic system; η depends on the outcome ω of a set of random parameters that describe the input and the system itself (as well as on other physical

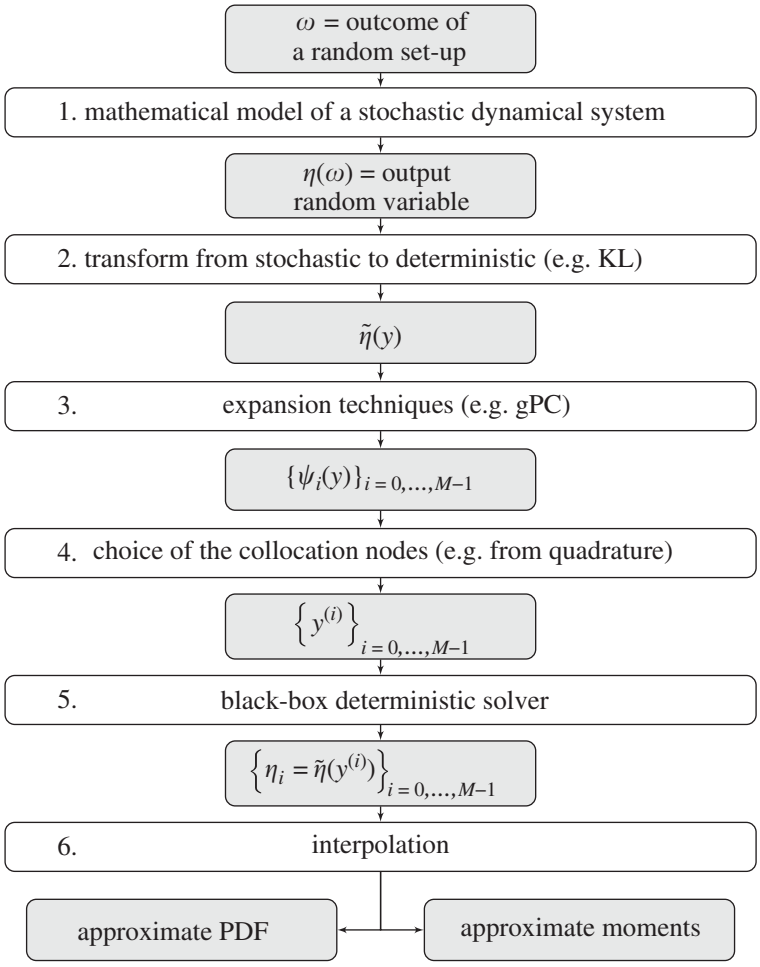

Fig. 1. Uncertainty quantification *via* gPC flow chart.

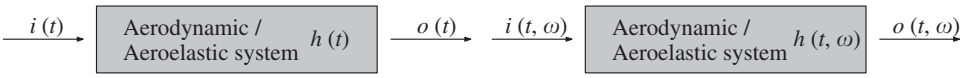

Fig. 2. (a) Deterministic and (b) stochastic systems.

variables, such as time, space, etc. which will not explicitly appear hereafter). The previous relationship can therefore be described by the map

$$\omega \mapsto \eta(\omega). \tag{1}$$

The analysis of (1) could be better afforded by introducing a dependence of the output random variable on a set of Q independent random variables $Y(\omega) = \{Y_1(\omega), Y_2(\omega), \ldots, Y_Q(\omega)\}$, with zero mean and unit variance (block 2), so that

$$\eta(\omega) = \tilde{\eta}(Y_1(\omega), Y_2(\omega), \ldots, Y_Q(\omega)) = \tilde{\eta}(Y(\omega)). \tag{2}$$

The random variables Y_q, $q = 1, \ldots, Q$, are called *input random variables*. In many cases, the parameters which describe the stochastic system can be naturally related to input random variables with the desired properties. When this is not possible, or when the laws of these parameters are known only through some of their statistics, in particular their covariance functions, the Karhunen–Loève (Loève, 1977) transform provides the mathematical tool to achieve this goal. One can expand η along an infinite sequence of independent variables $Y(\omega) = \{Y_1(\omega), Y_2(\omega), \ldots, Y_q(\omega), \ldots\}$, which is then truncated to a finite number, say Q, of terms.

In the following, we will rewrite Eq. (1) as

$$\omega \mapsto Y(\omega) \mapsto \tilde{\eta}(Y(\omega)), \tag{3}$$

and we concentrate on the second map which is in fact a (deterministic) function of real variables. At the same time, the first map in Eq. (3) is completely described by the knowledge of the laws of the input random variables. Posing

$$y = Y(\omega), \tag{4}$$

i.e., posing $y_q = Y_q(\omega)$ for $q = 1, \ldots, Q$, with y_q ranging in some interval $I_q \subseteq \mathbb{R}$, allows us to transform the stochastic dependence of the output random variable upon the random parameters of the system into a deterministic dependence of a function upon a set of real independent variables, i.e.,

$$y \mapsto \tilde{\eta}(y). \tag{5}$$

Here the interval I_q can be viewed both as the image of the random variable Y_q and as the domain of the deterministic map in the qth dimension.

Let us assume that the input random variables Y_q each admit a density ρ_q. A product density $\rho = \bigotimes_{q=1}^{Q} \rho_q$, i.e., $\rho(y) = \prod_{i=1}^{Q} \rho_q(y_q)$, for the vector of the input random variables Y immediately follows from independence. The probabilistic moments of the output random variable become deterministic integrals weighted by the density, as

$$\mathbb{E}[\eta^p] = \int_I \rho(y) \tilde{\eta}^p(y)\, \mathrm{d}y, \tag{6}$$

where $I = \prod_{q=1}^{Q} I_q$ is the so-called *stochastic domain*.

Once the laws of the input random variables are known, an efficient method must be employed to relate them to the output random variables in order to obtain the desired statistics of the latter. The most intuitive of these methods is represented by the classical MC approach (Caflisch, 1998), which is based on pseudo-random number generation: a set of realisations of the input random variables is generated according to their laws, a set of realisations of the output random variables is obtained through the corresponding deterministic systems and statistics are computed on the last set.

As an alternative, both the input and the output random variables can be represented through a (possibly infinite) linear combination of properly chosen "elementary" random variables (block 3); this approach allows an explicit

representation of the output random variables to be made, from which their moments and probability distribution can be obtained. The choice of the set of elementary random variables can dramatically influence the number of realisations required to obtain a sufficiently precise approximation of the output random variables. The expansions based on the (generalised) Polynomial Chaos approach, gPC (Ghanem and Spanos, 1991; Xiu and Karniadakis, 2002) exploit the classical technology of the weighted orthogonal polynomials. This leads to a very efficient choice of the required realisations whenever the map (5) is smooth. Such a kind of expansion generalises the classical Wiener (1938) approach which is based on an expansion in terms of Gaussian basis random variables. The form of the Gaussian density immediately leads to the use of Hermite polynomials, which are orthogonal with respect to it. When different laws are chosen for the basis random variables, as for gPC, different families of polynomials are introduced in order to guarantee orthogonality with respect to the corresponding density.

Interest is thus posed on giving an approximate representation of the random variable η. Classical results ensure that there always exists a family of polynomials

$$\{\varphi_k^{(q)}\}_{k\in\mathbb{N}},$$

which is orthonormal with respect to the weight function ρ_q. When this family is not one of the classical families of orthogonal polynomials (such as Legendre, Chebyshev, Hermite), i.e., when the density of the input random variables is not equal to the weight associated with a closed-form orthogonality relationship, approximate knowledge of the coefficients defining the three-term orthogonality recurrence relationship can still be obtained (Gautschi, 2004).

Next, through tensorisation, we obtain an orthonormal family of multivariate polynomials,

$$\{\varphi_k\}_{k\in\mathscr{K}}, \quad \mathscr{K}=\mathbb{N}^Q \text{ with } \varphi_k(y)=\prod_{q=1}^{Q}\varphi_{k_q}^{(q)}(y_q),$$

which forms the so-called (generalised) Polynomial Chaos. Thus, the gPC expansion of $\tilde{\eta}$ reads

$$\tilde{\eta}(y)=\sum_{k\in\mathscr{K}}\tilde{\eta}_k\varphi_k(y). \tag{7}$$

In view of the numerical treatment of random variables through their chaos representation, a truncation of the latter is introduced, say

$$\tilde{\eta}^M(y)=\sum_{i=0}^{M-1}\eta_i\Psi_i(y), \tag{8}$$

where $\Psi_i=\varphi_k$ for some $k=k(i)\in\mathscr{K}$ and M is the cardinality of a finite-dimensional orthonormal basis of a space of Q-variate polynomials. One possible choice is to introduce the space W_Q^P of the Q-variate polynomials of total degree at most P, which leads to

$$M=\binom{Q+P}{Q}.$$

The coefficients η_i of the truncated gPC expansion can be obtained by interpolation of the point-wise values of $\tilde{\eta}$ obtained from a set of M realisations $\{y^{(i)}\}_{i=0,\ldots,M-1}$ (block 4). This set is usually chosen as the set of nodes of a Gaussian or quasi-Gaussian quadrature rule. When the gPC expansion is made in terms of a nonclassical family of orthonormal polynomials, a nonclassical Gaussian quadrature rule can be obtained through numerical approximations (Gautschi, 2004). Gaussian quadrature is optimal in the sense of the highest possible polynomial exactness. When subsequent levels of approximations are required, for instance to evaluate convergence of the approximation procedure, a family of nested quadrature rules is however preferred, because of the reduction of the necessary expensive computations corresponding to each quadrature node. Among the nested quadrature families, Gauss–Patterson rules (Patterson, 1968) are once again optimal in the polynomial exactness sense. Each point-wise value $\tilde{\eta}(y^{(i)})$ can be obtained both through experimental tests and through computational simulations: the deterministic relationship between a single random input realisation and the corresponding random output can be considered as a black-box (block 5).

The approximate moments of the output random variable η can be directly obtained from the coefficients of the truncated gPC expansion. At the same time, an approximate form of the η probability density function (PDF) can be computed from the gPC interpolation (block 6). A possible method to achieve this goal is an *a posteriori* MC method: a set of realisations of the input random variables is obtained through quasi-random number generation. A sample of values of the output random variable then follows from the interpolation function. Finally, statistical approaches can be used to obtain an approximate probability density function from this sample.

The efficiency of the method comes from the properties of the orthogonal polynomial expansions: the spectral convergence leads to an exponential error reduction with respect to the polynomial degree, i.e., err $\propto \exp(-\gamma P)$. As a comparison, let us consider the classical form of the MC approach: the error depends on the number N of realisations as err $\propto 1/\sqrt{N}$. For instance, if a single input random variable is present, i.e., $Q=1$, and an error err$\sim 10^{-3}$ is required, the gPC expansion needs $M = P + 1 \sim 3 \log 10/\gamma$ realisations, while the MC approach needs $N \sim 10^6$ realisations. This advantage clearly decreases with the increase of the *stochastic dimension* Q, as the error of the MC does not depend on it and a more sophisticated form of the gPC approach must be employed to reduce the so-called *curse of dimensionality*.

The gPC approach introduced above makes use of a *global* expansion of the output random variables, i.e., an expansion which is the same over the whole stochastic domain I. On the other hand, an irregular or strongly varying dependence of the output upon the input variables would cause undesired oscillations in the global expansion. In these cases, a stochastic domain decomposition should be preferred, by defining gPC *local* expansions on subsets of I. The local expansions are then combined to return to a global representation of the output. This leads to the so-called Multi-Element generalised Polynomial Chaos, ME-gPC (Wan and Karniadakis, 2006b). A decomposition of the stochastic domain $I = \prod_{q=1}^{Q} [a_q, b_q]$ is introduced:

$$\begin{cases} I = \bigcup_{l=1}^{L} J_l, \\ J_l = [a_{l,1}, b_{l,1}] \times \cdots \times [a_{l,Q}, b_{l,Q}], \\ \text{measure}(J_{l_1} \cap J_{l_2}) = 0, \quad l_1 \neq l_2, \end{cases} \tag{9}$$

which leads to a decomposition of the outcome space. A new random variable $Y^{(l)}$ can be locally defined, subject to a conditional PDF,

$$\hat{\rho}(y^{(l)} | \chi_{J_l} = 1) = \frac{\rho(y^{(l)})}{\mathscr{P}(\chi_{J_l} = 1)}, \tag{10}$$

in each *random element* J_l. A local polynomial approximation $\tilde{\eta}_l^M(y^{(l)})$ can then be introduced for each random element J_l, using an orthogonal system $\{\varphi_k^{(l)}(y^{(l)})\}$, with respect to the local conditional PDF $\hat{\rho}$. The approximation of the entire random field can finally be recovered from the local approximations as

$$\tilde{\eta}^L(y) = \sum_{l=1}^{L} \tilde{\eta}_l^M(y) \chi_{J_l}(y) = \sum_{l=1}^{L} \sum_{i=0}^{M_l - 1} \eta_i^{(l)} \Psi_i^{(l)}(y) \chi_{J_l}(y). \tag{11}$$

The entire ME-gPC approximation procedure can be represented in a flowchart similar to the one in Fig. 1, with the blocks from 3 to 6 repeated for each stochastic element J_l, and a final global solution reconstruction step before the approximate PDF and moments of the output random variables are obtained.

3. Deterministic evaluation of the aerodynamic and aeroelastic behaviour

The so-called black-box solver (block number 5 in the gPC flowchart in Fig. 1) depends on the application of interest. The aerodynamic application exclusively requires a computational model devoted to the simulation of the fluid flow around the obstacle. The aeroelastic application instead needs an additional component, that is, the identification procedure adopted to determine the flutter derivatives using the obtained computational results.

As regards the first common component, the incompressible, unsteady, 2-D laminar flow is modelled through the Arbitrary Lagrangian–Eulerian (ALE) version (Nomura and Hughes, 1992) of the classical Navier–Stokes equations. It is worth pointing out that the adopted flow model is not suitable for $\mathrm{Re} < 10$ or $\mathrm{Re} > 5 \times 10^5$, when compressibility and turbulence effects take place. From a general point of view, different flow models could be adopted in the black-box solver if required by the Re values, i.e., by the choice of the considered collocation nodes. Nevertheless, the application carried out in the present study only involves collocation nodes in the laminar range, where the adopted flow model applies. Dirichlet conditions are imposed on the velocity at the inlet as well as Neumann conditions on the stress tensor at the outlet. No-slip conditions are retained at the plate wall, along with impulsive initial conditions in the inside of the fluid domain. The motion of the plate boundary, i.e., of the fluid boundary, is imposed *a priori* following the smoothed ramp motion of the rotational centre of the plate. As the computational domain boundary depends on time, the computational grid needs to be modified according to the boundary motion (dynamic mesh) (Batina, 1989). A spring analogy method is employed to this aim. The approximate numerical solution of the equations is provided through the Finite Volume Method (FVM), (Ferziger and Peric, 2002), using FLUENT® commercial software.

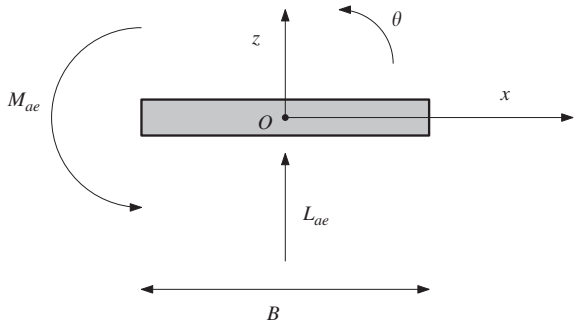

Fig. 3. Reference system.

Advancement in time is accomplished using the first-order implicit Euler scheme. The cell-centre values of the variables are interpolated at face locations using a second-order central difference scheme for the diffusive terms. The interpolation of the convection terms is accomplished by means of the Quadratic Upwind Interpolation for Convective Kinematics (QUICK) on quadrilateral cells, while the second-order upwind scheme (2UPW) is employed on triangular cells.

As far as the aeroelastic transfer function identification is concerned, the motion-induced aeroelastic forces can be expressed according to the Scanlan and Tomko model, reported in Simiu and Scanlan (1996):

$$L_{ae} = \frac{1}{2}\rho U^2 B\left[\frac{1}{U_r}H_1^*\left(\frac{1}{U_r}\right)\frac{\dot{z}}{U} + \frac{1}{U_r}H_2^*\left(\frac{1}{U_r}\right)\frac{B\dot{\theta}}{U} + \frac{1}{U_r^2}H_3^*\left(\frac{1}{U_r}\right)\theta + \frac{1}{U_r^2}H_4^*\left(\frac{1}{U_r}\right)\frac{z}{B}\right] \tag{12}$$

and

$$M_{ae} = \frac{1}{2}\rho U^2 B^2\left[\frac{1}{U_r}A_1^*\left(\frac{1}{U_r}\right)\frac{\dot{z}}{U} + \frac{1}{U_r}A_2^*\left(\frac{1}{U_r}\right)\frac{B\dot{\theta}}{U} + \frac{1}{U_r^2}A_3^*\left(\frac{1}{U_r}\right)\theta + \frac{1}{U_r^2}A_4^*\left(\frac{1}{U_r}\right)\frac{z}{B}\right], \tag{13}$$

where L_{ae} and M_{ae} are the lift force and the pitching moment evaluated at the pole $O(0.5B;0)$, ρ the air density, U the incoming flow velocity, B the obstacle chord, U_r the reduced velocity and z and θ are the heave and pitch components of the displacement of pole O, respectively (Fig. 3). The coefficients $H_i^*(1/U_r)$ and $A_i^*(1/U_r)$ are called *flutter derivatives*.

In this paper, the flat plate flutter derivatives are evaluated through the quasi-indicial approach introduced by Fransos and Bruno (2006). The unsteady flow-field around the flat plate, subject to a smoothed ramp motion, is numerically computed and the unsteady forces acting on the plate itself are obtained. The hypothesis of aeroelastic system linearity allows the inputs and the outputs of the system itself to be decomposed through a frequency analysis. This decomposition leads to the identification of the flutter derivatives at each frequency (i.e., each reduced velocity) for which the frequency content of the input is sufficiently high. The approach results in a very efficient algorithm that allows the identification of the flutter derivatives in the whole reduced velocity range of interest through only a single computational flow-field evaluation for each degree of freedom.

4. Stochastic characterisation of the steady flow around the motionless plate

The stochastic characterisation of the steady flow around the motionless plate focuses on both the drag coefficient and flow field quantities. The former has been accounted for as an output random variable in two sensitivity studies, both related to the choice of the collocation nodes (block 4 in the gPC flowchart in Fig. 1).

4.1. Sensitivity analysis to the interpolation polynomial degree

The single input random variable retained in the following analysis is the Reynolds number $Y = \mathrm{Re} = UB/\nu$, where ν is the kinematic air viscosity and the chord value is set equal to $B = 0.1$ m. Hence, the Reynolds number depends in turn

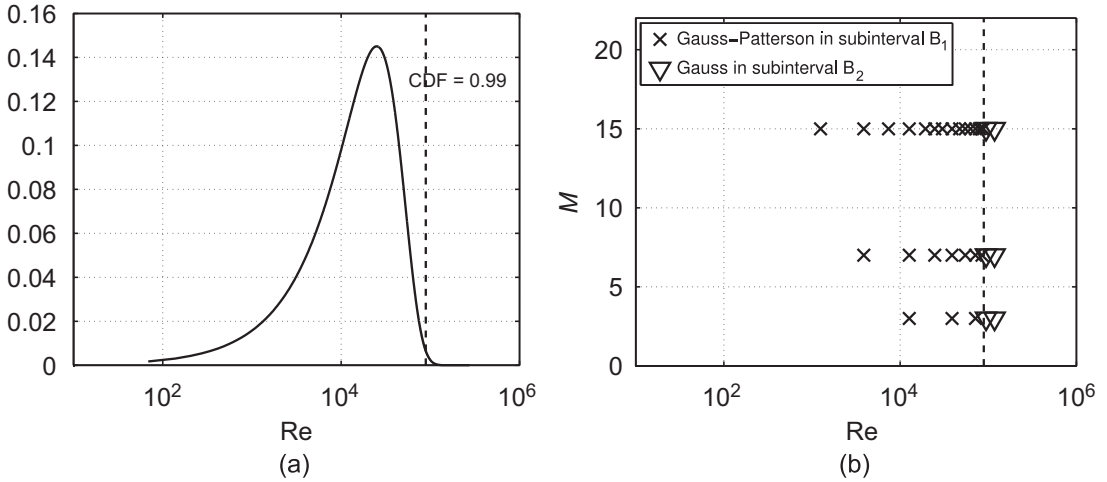

Fig. 4. (a) Weibull PDF for Re and (b) corresponding ME-gPC quadrature nodes.

on the random variable U, i.e., the incoming mean wind speed, defined on the probability space $(\Omega, \mathscr{F}, \mathscr{P})$. The law of U is derived from statistics arguments based on on-site measurements of the wind velocity at Schipol, The Netherlands (Troen and Petersen, 1989). The $Y = \mathrm{Re}$ Weibull(α,β) PDF

$$\rho(y) = \beta\alpha^{-\beta}(y)^{\beta-1}\exp(-(y/\alpha)^{\beta}), \quad \alpha = 5.6, \quad \beta = 1.83, \tag{14}$$

best fits the experimental data. Its support is $I = [0, +\infty)$, but the Cumulative Distribution Function (CDF) reaches the value CDF $= 0.99$ already at $\mathrm{Re} = 8.9 \times 10^4$, as shown in Fig. 4(a). Employing a gPC expansion on the whole support of the input PDF could lead to placing many collocation points in the tail, if a high order gPC is employed. The use of a ME-gPC approach (Wan and Karniadakis, 2006b) prevents this from happening and allows a low order quadrature rule to be fixed in the tail and the use, for instance, of a nested family of quadrature rules in the interval of greatest probability content in order to obtain subsequent levels of approximation. The partition

$$I = [0, +\infty) = [0, 8.9 \times 10^4] \cup [8.9 \times 10^4, +\infty) = J_1 \cup J_2$$

is used in the following. One conditional PDF is therefore associated to each of the input random variables $Y^{(1)}$ and $Y^{(2)}$ in the two subdomains, as in Eq. (10).

A family of orthogonal polynomials exists in both subintervals, with respect to the corresponding conditional PDF. Hence, Gaussian and quasi-Gaussian quadrature formulas can be constructed with respect to the weight function defined by the PDF (Gautschi, 2004). A family of nested Gauss–Patterson rules is associated to the subinterval B_1. The computation of the 3-point, 7-point and 15-point rules is performed in quadruple precision (Patterson, 1989, Fig. 4(b)). Stability issues with Patterson's algorithm are highlighted when passing to the higher order rules. A 2-point Gauss formula is employed in the second subinterval B_2. Note that all the nodes lie in the $10 < \mathrm{Re} < 5 \times 10^5$ range, which corresponds to a laminar flow.

Local gPC approximations are introduced in both subintervals in terms of PC interpolant $I_M\eta(y) = \tilde{\eta}^M(y)$, where $\eta(y)$ is the generic output random variable of interest, according to Section 2. Here, the drag coefficient C_D is taken as the output random variable of the problem. Each realisation, corresponding to a quadrature node, is given by the numerical simulation of the steady flow-field around the motionless plate and the subsequent integration which leads to the resulting force acting on the plate. When local approximations are obtained in each of the stochastic subdomains B_1 and B_2, a global approximation immediately follows.

Fig. 5(a) shows the PC interpolation of the C_D computed values for three different levels of approximation. It should be noticed that the ME-gPC interpolants are defined over the whole stochastic domain I. These are possibly discontinuous polynomials composed of one of the $I_M C_D(y^{(1)})$ interpolants in the Gauss–Patterson quadrature nodes over the B_1 subdomain and by the 2-point $B_2 C_D(y^{(2)})$ interpolant in the two Gauss quadrature nodes over the

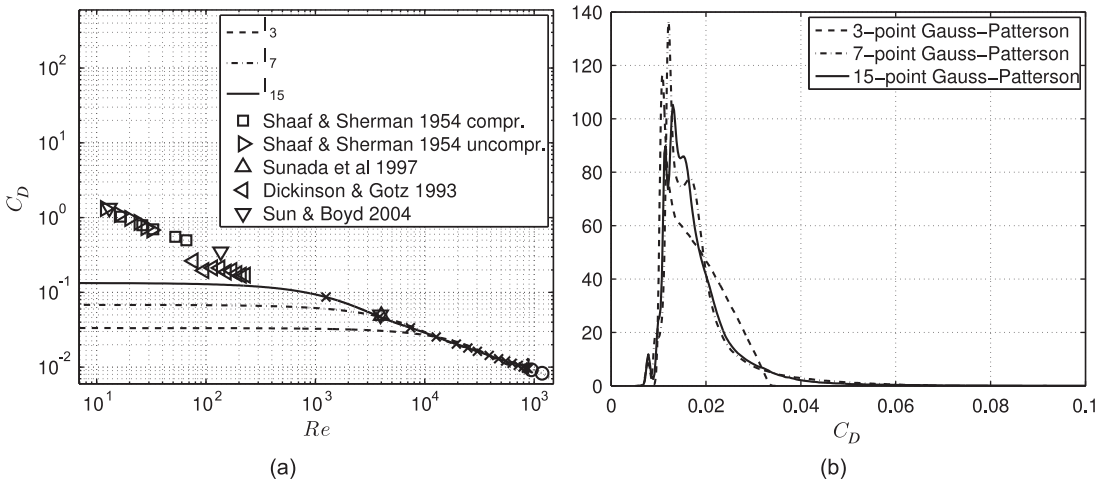

Fig. 5. (a) Drag coefficient PC interpolation and (b) approximate PDF.

Table 1
Moments and fractiles.

	Mean	Variance	0.99-percentile
3	1.763×10^{-02}	3.323×10^{-05}	3.122×10^{-02}
7	1.813×10^{-02}	6.312×10^{-05}	5.051×10^{-02}
15	1.824×10^{-02}	7.832×10^{-05}	5.411×10^{-02}

B_2 subdomain. The increasing precision of the higher order Gauss–Patterson formulas is highlighted, showing the need for a relatively large number of collocation nodes. For such a reason, the use of nested quadrature rules could be profitable, as they offer the opportunity of estimating the obtained accuracy with the addition of a sufficiently small number of nodes.

Similar considerations can be made about the approximate PDFs that result from the ME-gPC interpolants (Fig. 5(b)): the 3-point Gauss–Patterson rule leads to a poor approximation of the PDF over the whole C_D range. In particular, an inadequate description of the PDF tail is obtained and, in turn, an underestimation of the highest percentiles. The 7-point and 15-point rules give approximations which are much closer to each other, and this is an index of a satisfactory convergence of the stochastic solution procedure. The presence of very thin peaks is not related to a physical multi-modality, but to small oscillations in the interpolant polynomial due to its high order and to the statistical PDF estimation method. These peaks should be considered more as numerical approximation errors.

Table 1 shows the first two approximate statistical moments (mean and variance) and the approximate value of the 0.99-percentile for the three different levels of approximation. These numerical values are obviously related to the approximate PDF and they are important in that they represent the main final stochastic design parameters that engineers can read from the stochastic analysis procedure. Once again, large differences can be noticed between the 3-point and the 7-point approximations, while the latter and the 15-point approximation are much closer (less than 7%). It follows that a sufficient level of approximation has been reached and the 15-point interpolation in the main probability subdomain is retained as the approximation level in the following sections.

4.2. Sensitivity analysis to large gradients in low probability density regions

Fig. 5(a) shows that the experimental data (Schaaf and Sherman, 1954; Dickinson and Gotz, 1993; Sunada et al., 1997; Sun and Boyd, 2004) in the $\mathrm{Re} < 400$ region are badly fitted by the proposed ME-gPC interpolation. This is

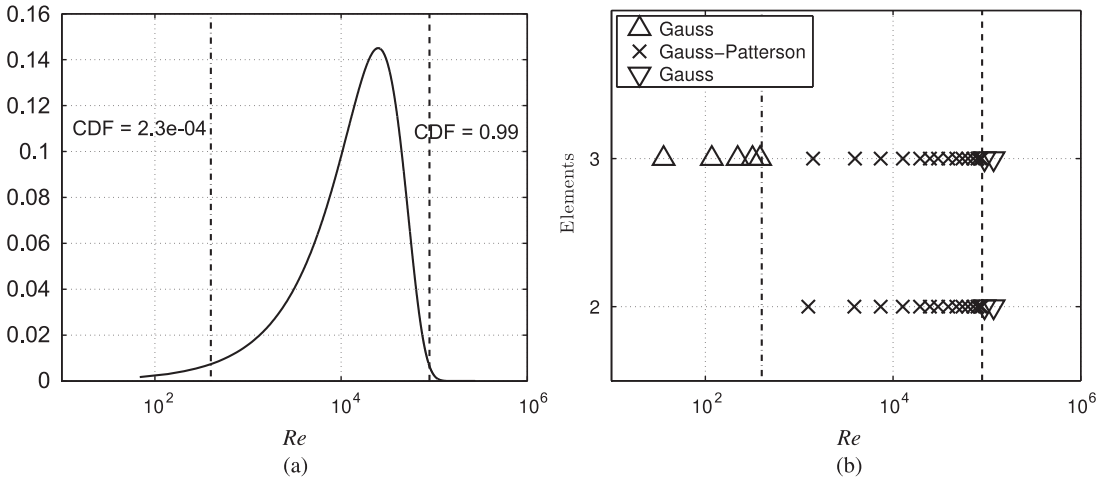

Fig. 6. (a) Weibull PDF for Re and (b) corresponding ME-gPC quadrature nodes.

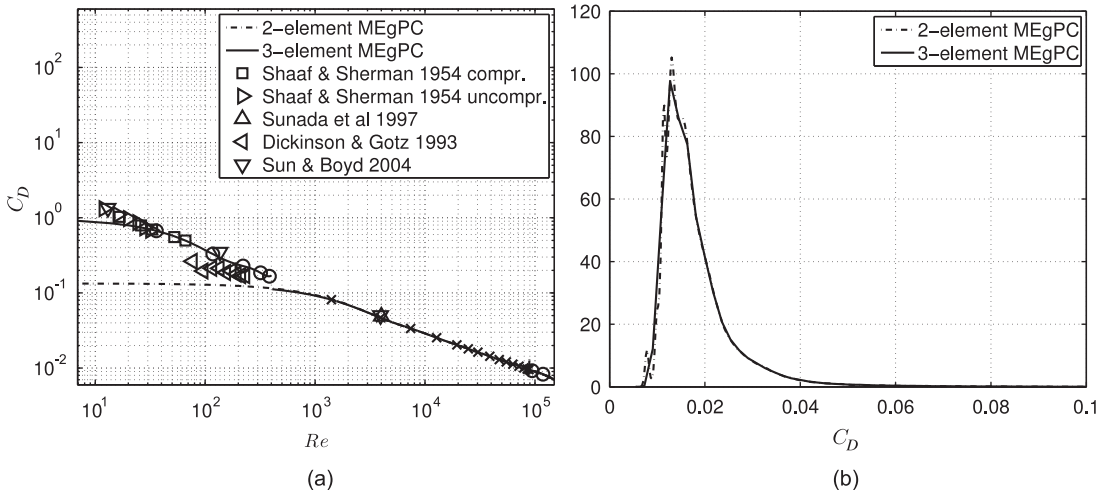

Fig. 7. (a) Drag coefficient PC interpolation and (b) approximate PDF.

not surprising, because this region contains a change in the physical regime, as already pointed out by Bruno and Fransos (2008). At the same time, the probability that the input random variable Re is in that region is only 2.3×10^{-4}. The aim of this section is to evaluate the effect of an improved approximation in this region on the output quantities of interest.

Let us introduce a partition of the stochastic domain I into three subdomains, in an analogous manner to what was done in Section 4.1. Here, we have $I = [0, 4 \times 10^2] \cup [4 \times 10^2, 8.9 \times 10^4] \cup [8.9 \times 10^4, +\infty) = J'_1 \cup J'_2 \cup J'_3$, as shown in Fig. 6(a). This new stochastic domain partition leads to a three-element ME-gPC approximation (3-el.). In the J'_2 interval, i.e., the subdomain corresponding to the large amount of probability density, a nested family of Gauss–Patterson quadrature rules is employed. The 15-point rule is retained for comparison with the above two-element (2-el.) ME-gPC approximation. The same two-point Gauss rule as before is employed in the right tail, i.e., J'_3. A five-point Gauss rule is introduced in the left tail, to better fit the data in this region. A comparison of the two and three-element collocation node sets is given in Fig. 6(b). Gauss and Gauss–Patterson optimality is given by the fact that their nodes are distributed according to the weight function of the integral they are intended to approximate: this

Table 2
Moments and fractiles.

	Mean	Variance	0.99-percentile
2-Elements	1.824×10^{-02}	7.832×10^{-05}	5.411×10^{-02}
3-Elements	1.824×10^{-02}	8.518×10^{-05}	5.329×10^{-02}

consideration, along with the similar density content of J_1 and J_2', makes the very slight difference between the Gauss–Patterson nodes in those intervals obvious.

The corresponding ME-gPC interpolation of C_D is given in Fig. 7(a). The discontinuous nature of the piece-wise polynomial interpolation is shown by the three-element interpolant behaviour. The three different polynomials give a good fitting of the experimental and computational data in all the regimes in this case. This better interpolation, however, does not result in a significantly different C_D stochastic characterisation. The approximate PDFs of the two- and three-element cases are plotted in Fig. 7(b) to support this statement. The resulting PDFs are very similar, as the C_D values corresponding to the highest probability lie in the range corresponding to the Gauss–Patterson related regions. Similarly, the two first statistical moments (mean and variance) and the 0.99-percentile, which are shown in Table 2, do not significantly vary between the two- and three-element approximations. The two-element ME-gPC is therefore retained in the following for the stochastic characterisation of other output quantities of interest.

4.3. Stochastic description of the flow field

The drag coefficient C_D does not completely characterise the steady flow-field around the motionless plate. Other physical quantities can be chosen as output random variables to complete the stochastic description of the flow-field. Among all the possible choices, the friction coefficient C_f along the lateral wall of the plate and the horizontal velocity u_x in the plate wake are considered in the following, analogously to what was done in Bruno and Fransos (2008).

An alternative representation of the stochastic output, the boxplot representation, may be preferred when dealing with stochastic outputs that depend on variables other than the stochastic ones (for instance space, as in this case). A statistical sample of the values of the output random variables at given points in the physical space is obtained through random number generation of the gPC basis random variables. The plot of the lower quartile, median, and upper quartile values, along with two lines posed 1.5 times the interquartile range (difference between the third and the first quartile) above and below the upper and lower quartile, respectively, can then be obtained from each of these samples.

A boxplot of the C_f at some points along the upper surface of the plate is given in Fig. 8(a). The deterministic C_f distributions at $\mathrm{Re} = 10$ and 10^5 are plotted for reference. The mean value has a trend versus x/B analogous to the deterministic spatial profiles. The C_f mean value distribution is much closer to the high Re deterministic distribution than to the low Re one: this reflects the Re input random variable PDF. The higher C_f moments are very similar all along the surface: for instance, the variance varies along the lateral surface in the $[7.7 \times 10^{-06}, 4.6 \times 10^{-05}]$ range. Hence, the approximate PDF at $x/B = 0.5$, i.e., at mid-plate, is chosen as representative in Fig. 8(b). Its shape is close to the Weibull PDF of the random input: this implies a strong nonsymmetry; in fact, the average of the skewness values along the surface is equal to 8.6987.

The horizontal velocity u_x along the $z/B = 0$ line in the wake is also stochastically represented through a boxplot in Fig. 8(c). The profile of the mean value distribution is close to the classical Goldstein solution [see, e.g., Schlichting (1979)], which is plotted here for reference. The variance is shown to rapidly decrease moving downstream: this is due to the fact that, in an analogous manner to the deterministic analysis in Bruno and Fransos (2008), the Re sensitivity of the boundary layer thickness locally affects the near wake velocity defect, while the Re sensitivity strongly decays at a distance far downwind. The u_x boxplot representation also suggests a more symmetrical statistical distribution than the C_f one all along the wake. This is confirmed by a much lower value of the skewness, whose average along x/B is now equal to 1.8706. Hence, the PDF profile is much closer to a Gaussian one; the approximate PDF at $x/B = 1.5$ is plotted in Fig. 8(d) as an example. Once again, the oscillations in the resulting PDF around $u_x/U = 0.67$ should be ascribed to small oscillations due to the high order of the interpolant polynomial.

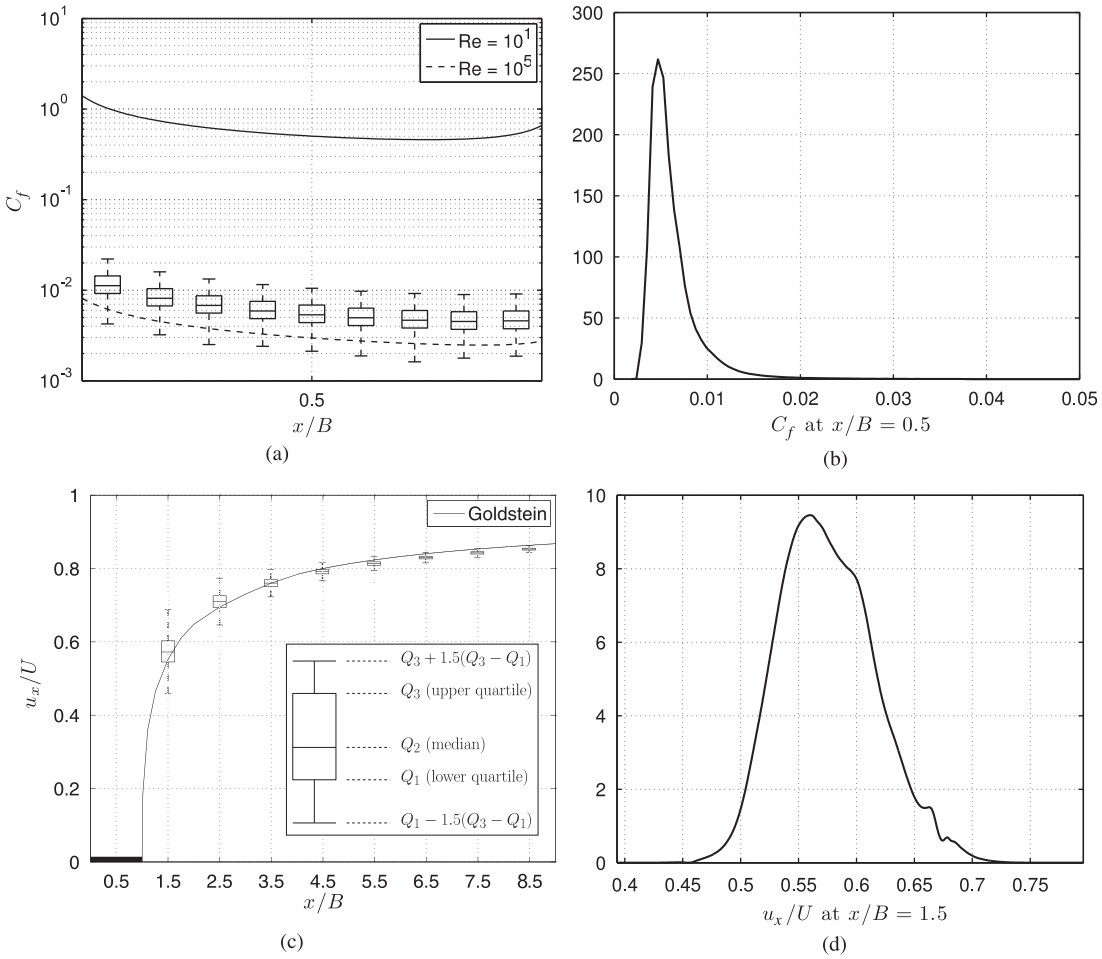

Fig. 8. Friction coefficient at the upper surface: (a) boxplot stochastic representation and (b) approximate PDF at $x/B = 0.5$; (c) horizontal velocity at $y/B = 0$.

5. Stochastic characterisation of the unsteady flow around the moving plate

The flutter derivatives, at different fixed reduced velocities U_r, are taken as the output random variables of the problem in this section. From the mathematical point of view, it is worth pointing out that, even though the black-box solver proceeds to the flutter identification through the frequency analysis of time-dependent deterministic forces, the obtained flutter derivatives are not time-dependent. Thus, the subsequent stochastic characterisation of the flutter derivatives does not require the gPC description of time-dependent random processes and hence does not involve long term integration, which is well known as a critical point (Wan and Karniadakis, 2006a).

5.1. Sensitivity analysis to the interpolation polynomial degree

The two-element ME-gPC approximation is performed for the complete set of flutter derivatives in the $0 \leq U_r \leq 12$ range of interest. Three different interpolants I_3, I_7 and I_{15} are taken into account in the J_1 element to evaluate the possible need for a high level of approximation, in analogy to what has been done in Section 4.1. Fig. 9 shows the three interpolants for each flutter derivative at $U_r = 2$. The increasing precision of the higher order Gauss–Patterson formulas is highlighted once again, even though small oscillations appear in proximity to the J_1 subdomain upper bound for certain derivatives (e.g., H_1 and A_2), due to the high polynomial degree. As regards the computational costs,

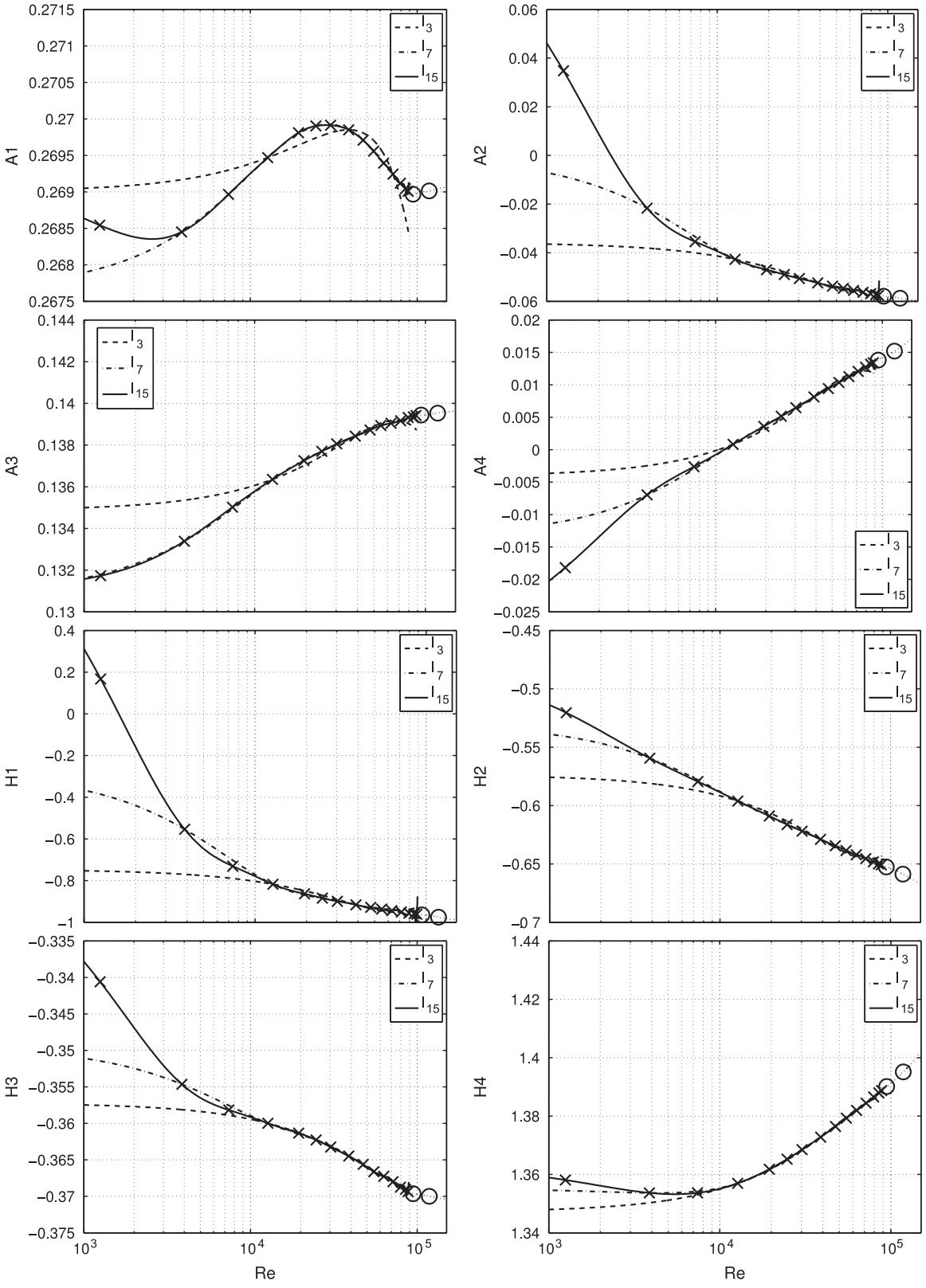

Fig. 9. ME-gPC interpolation for the flutter derivatives at $U_r = 2$.

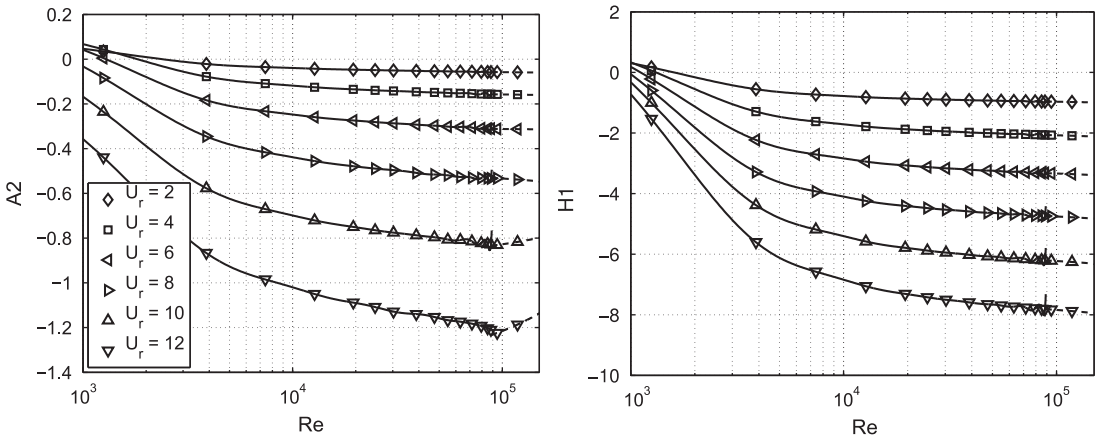

Fig. 10. PC interpolation for the flutter derivatives at different U_r.

a relatively large number of collocation nodes is also needed in the unsteady case, and, in addition, the evaluation cost of a single collocation node is much higher than in the steady case: the use of nested quadrature rules is therefore crucial, if subsequent levels of approximation are required.

The A_2 and H_1 flutter derivatives mainly contribute to the aeroelastic damping and are clearly recognised as the most significant ones in the characterisation of the aeroelastic system. Their 15-point interpolants are plotted in Fig. 10 at a large number of reduced velocities, showing a good overall description of the derivatives as functions of Re.

It is worth pointing out that the A_1 and H_3 derivatives show a different trend in the Re range roughly corresponding to the J_2 element at $U_r = 2$ (Fig. 9). The same happens for other derivatives at higher reduced velocities (for instance A_2 at $U_r = 10, 12$ in Fig. 10). This change in the derivative trend can be ascribed to a different flow regime in the wake. In fact, the plate motion causes the shedding of a vortex from the plate trailing edge, which represents a perturbation of the flow in the wake. Bearing in mind that the Re effects on such a perturbation can be much more significant at a distance far downstream in the wake due to diffusion, it can have more effect on the long nondimensional wavelengths λ or, in other terms, the high reduced velocities $U_r = UB/f = U\lambda$. This fact could explain why, for instance, the A_2 derivative in Fig. 10 only reveals a change in trend at $U_r \geq 10$. Finally, the same phenomenon is not shown by the computational simulation performed for the motionless plate: no flow perturbations are introduced in this case, due to the absence of motion of the obstacle, and the only expected change in the flow regime is the laminar to turbulent transition along the plate surface; it is well known that transition occurs for this flow at a higher local Re value than the one corresponding to the last considered quadrature node.

5.2. Stochastic flutter derivatives

Once the interpolation has been performed for each flutter derivative at each reduced velocity of interest, the statistical representation of the derivatives is accomplished. Once again, three graphical representations can be made. Bearing in mind that the flutter derivatives do not depend only on the input random variable Y, but also on the (deterministic) reduced velocity U_r, Fig. 11 diagrams the boxplot representation for each derivative at six U_r samples and compares the obtained stochastic solution to the well-known deterministic Theodorsen solution. A more compact, yet incomplete, description of the derivative statistics is provided, in Fig. 12, by the mean value and variance evolutions versus U_r. Finally, Fig. 13 details the PDF at the sampled U_r values referring to the most significant derivatives, i.e., A_2 and H_1.

Two main considerations can be drawn:

(i) the Theodorsen solution, which is analytically obtained under the assumption of inviscid flow, always lies in proximity to the PDF tail (Fig. 11), that is, it is approached at high Re values as expected;
(ii) the higher the reduced velocity, the higher the variance of each derivative, except for H_4. A closer link between the derivative statistics and the fluid flow phenomena can be established bearing in mind that high U_r values in the frequency domain correspond to high values of the nondimensional unit $s = tU/B$ in the time or space domain: in

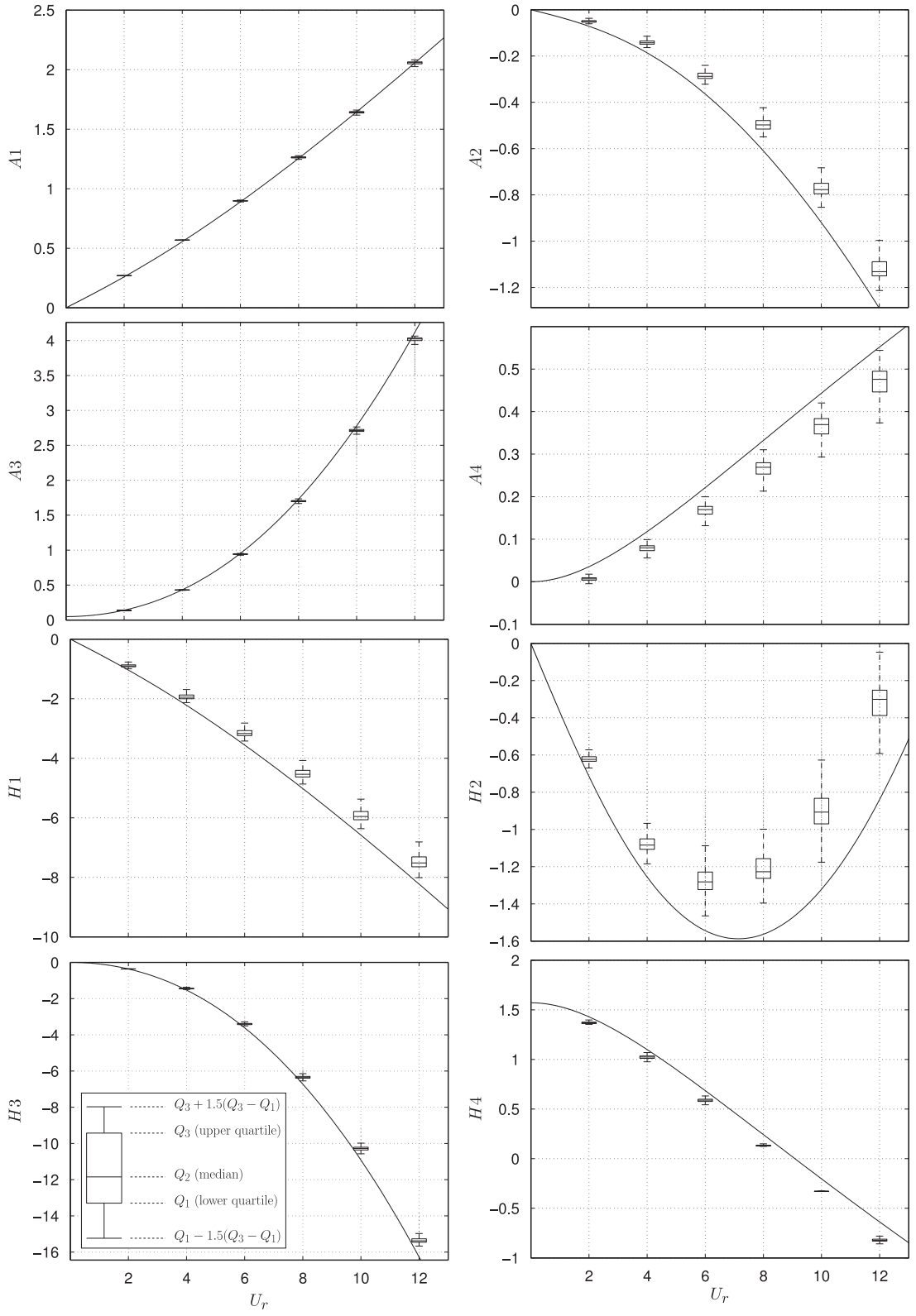

Fig. 11. Boxplots of the approximate flutter derivatives at different U_r. The solid line is the Theodorsen deterministic solution.

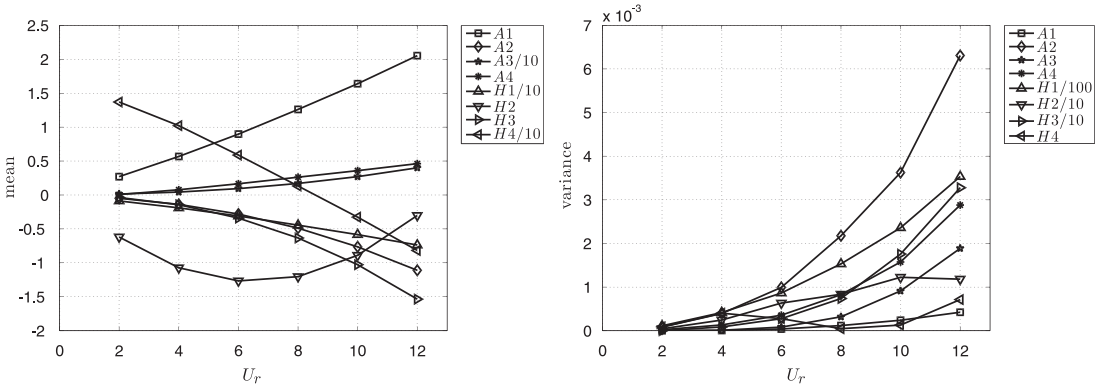

Fig. 12. Moments of the approximate flutter derivatives at different U_r.

other words, s can be viewed as a measure of the distance travelled by the vortex along the wake, or of the vortex travel time. Hence, the higher U_r, the longer the travel time and the stronger the diffusive effects involved by the kinematic viscosity, that is, by the Re effects.

The stochastic characterisation of the flutter derivatives allows us to obtain the probability that one of them is positive at some values of U_r; this probability is plotted in Fig. 14 for $A2$ and $H1$. A very low, but not null, probability is shown: a negative aeroelastic damping is therefore also possible for the flat plate, in contrast with the classical inviscid Theodorsen theory.

5.3. Computational costs

The combined use of different techniques from both numerical analysis and wind engineering was aimed at performing a complete stochastic analysis of the aerodynamic and aeroelastic problem with an affordable computational cost.

In particular, it is worth pointing out that the extraction method proposed for the flutter derivatives in Section 3 allows an efficient stochastic characterisation of the plate aeroelasticity. Only one single deterministic computation is in fact needed for the realisations of all the flutter derivatives that correspond to a spatial degree of freedom at each U_r value in the range of interest. This dramatically reduces the computational costs required for a complete stochastic analysis of the aeroelastic phenomenon. The gain, in terms of the required CPU time, can be observed in Fig. 15, which shows a comparison between the computational costs related to the harmonic oscillations and the smoothed ramp methods (Fransos and Bruno, 2006). The cost of the harmonic oscillation method refers to the classical 6-point sampling of the reduced velocity interval. The cost required for the employment of an accurate 15-point quadrature rule with the proposed smoothed ramp method is about one-half of that required for the employment of a less accurate 3-point quadrature rule with the harmonic oscillation method.

6. Conclusions

The present paper deals with the uncertainty quantification of the aerodynamic and aeroelastic behaviour of a streamlined body immersed in a viscous fluid flow. The classical flat plate problem has been addressed to this aim. The mean flow incoming velocity, and therefore the Reynolds number, has been retained as an input random variable.

A Multi-Element generalised Polynomial Chaos method, along with an efficient deterministic computational approach, has been proposed to obtain accurate approximations of the output random variables at an affordable cost. A stochastic characterisation of both the steady flow around the motionless plate and the plate flutter derivatives has been given, in terms of moments, percentiles, boxplots and approximate PDFs of the desired quantities.

The sensitivity of the resulting random outputs to both the polynomial interpolation degree and the presence of large gradients in low probability density regions has been investigated. The former study shows the need for a moderately

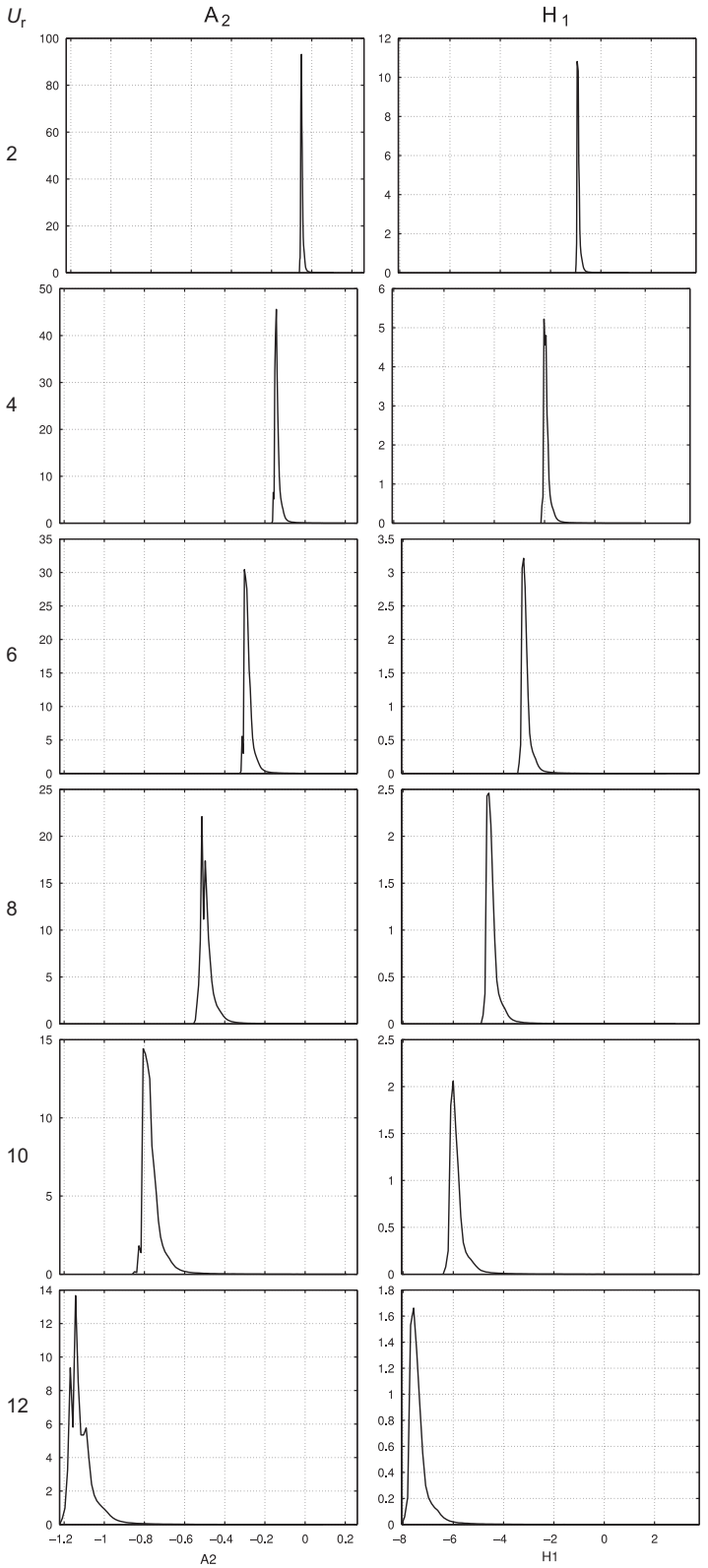

Fig. 13. PC-approximate PDFs for the flutter derivatives at different U_r.

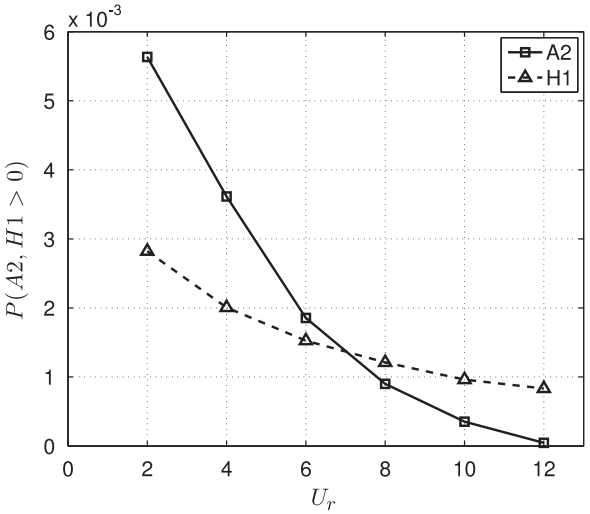

Fig. 14. Positive value probability for $A2$ and $H1$.

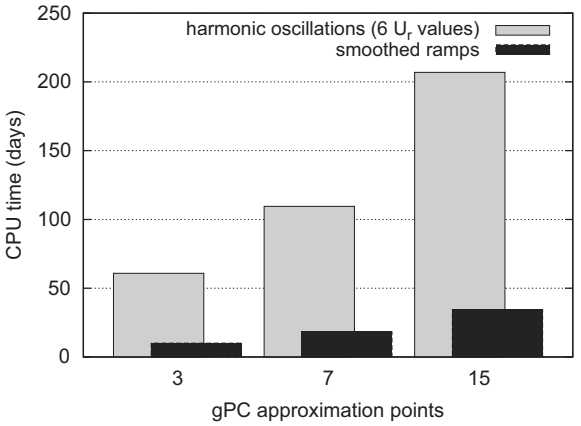

Fig. 15. Computational costs required for the harmonic oscillation and the smoothed ramp methods.

high number of collocation nodes and highlights the importance of an efficient deterministic method to evaluate the single realisations, in order to reduce the required computational costs. The latter sensitivity investigation shows that a good point-wise description of the stochastic solution in the low probability regions is not necessary for an accurate stochastic output description.

The overall resulting computational costs are affordable for real world applications. The obtained results highlight a nonzero probability of $A2$ and $H1$ of being positive, showing that a negative aeroelastic damping is possible for the flat plate, which is in contrast with the classical inviscid theory.

References

Babuška, I., Nobile, F., Tempone, R., 2007. A stochastic collocation method for elliptic partial differential equations with random input data. SIAM Journal on Numerical Analysis 45 (3), 1005–1034.

Batina, J.T., 1989. Unsteady Euler airfoil solutions using unstructured dynamic meshes. AIAA Paper 89-0115

Beloiu, D.M., Ibrahim, R.A., Pettit, C.L., 2005. Influence of boundary conditions relaxation on panel flutter with compressive in-plane loads. Journal of Fluids and Structures 21, 743–767.

Bruno, L., Fransos, D., 2008. Evaluation of Reynolds number effects on flutter derivatives of a flat plate by means of a computational approach. Journal of Fluids and Structures 24, 1058–1076.
Caflisch, R.E., 1998. Monte carlo and quasi-Monte Carlo methods. Acta Numerica 1–49.
Canuto, C., Fransos, D., 2009. Numerical solution of partial differential equations in random domains: an application to wind engineering. Communications in Computational Physics 5, 515–531.
Canuto, C., Kozubek, T., 2007. A fictitious domain approach to the numerical solution of PDEs in stochastic domains. Numerische Mathematik 107 (2), 257–293.
Deb, M.K., Babuška, I.M., Oden, J.T., 2001. Solution of stochastic partial differential equations using Galerkin finite element techniques. Computer Methods in Applied Mechanics and Engineering 190 (48), 6359–6372.
Dickinson, M.H., Gotz, K.G., 1993. Unsteady aerodynamic performance of model wings at low Reynolds number. Journal of Experimental Biology 174, 45–64.
Ferziger, J.H., Peric, M., 2002. Computational Methods for Fluid Dynamics, third ed. Springer, Berlin.
Fransos, D., Bruno, L., 2006. Determination of the aeroelastic transfer functions for streamlined bodies by means of a Navier–Stokes solver. Mathematical and Computer Modelling 43 (5–6), 506–529.
Gautschi, W., 2004. Orthogonal Polynomials: Computation and Approximation. Numerical Mathematics and Scientific Computation. Oxford University Press, New York.
Ghanem, R.G., Spanos, P.D., 1991. Stochastic Finite Elements: A Spectral Approach. Springer, New York.
Halfman, R., 1952. Experimental aerodynamic derivatives of a sinusoidally oscillating airfoil in two dimensional flow. NACA Technical Report 1108.
Kleiber, M., Hien, T.D., 1992. The Stochastic Finite Element Method. Basic Perturbation Technique and Computer Implementation. Wiley, Chichester.
Le Maître, O.P., Scanlan, R.H., Knio, O.M., 2003. Estimation of the flutter derivatives of an NACA airfoil by means of Navier–Stokes simulation. Journal of Fluids and Structures 17, 1–28.
Lindsley, N.J., Pettit, C.L., Beran, P.S., 2006. Non linear plate aeroelastic response with uncertain stiffness and boundary conditions. Structure and Infrastructure Engineering 2, 201–220.
Loève, M., 1977. Probability Theory, fourth ed. Springer, New York.
Mathelin, L., Hussaini, M.Y., Zang, T.A., 2005. Stochastic approaches to uncertainty quantification in CFD simulations. Numerical Algorithms 38, 209–236.
Nomura, T., Hughes, T.J.R., 1992. An arbitrary Lagrangian–Eulerian finite element method for interaction of fluid and a rigid body. Computer Methods in Applied Mechanics and Engineering 95, 115–138.
Patterson, T.N.L., 1968. The optimum addition of points to quadrature formulae. Mathematics of Computation 22, 847–856 (addendum, Mathematics of Computation 22 (104, loose microfiche supp.) C1–C11).
Patterson, T.N.L., 1989. Algorithm 672: generation of interpolatory quadrature rules of the highest degree of precision with preassigned nodes for general weight functions. ACM Transactions on Mathematical Software 15 (2), 137–143.
Pettit, C.L., 2004. Uncertainty quantification in aeroelasticity: recent results and research challenges. Journal of Aircraft 41 (5), 1217–1229.
Poirel, D., Price, S.J., 2003. Random binary (coalescence) flutter of a two-dimensional linear airfoil. Journal of Fluids and Structures 18, 23–42.
Sarkar, S., Bijl, H., 2008. Nonlinear aeroelastic behavior of an oscillating airfoil during stall induced vibration. Journal of Fluids and Structures 24, 757–777.
Sarkar, S., Witteveen, J.A.S., Loeven, A., Bijl, H., 2009. Effect of uncertainty on the bifurcation behavior of pitching airfoil stall flutter. Journal of Fluids and Structures 25, 304–320.
Schaaf, S.A., Sherman, F.S., 1954. Skin friction in slip flow. Journal of Aeronautical Sciences 21, 85–90.
Schlichting, H., 1979. Boundary-layer Theory, seventh ed. McGraw-Hill, New York.
Schwab, C., Todor, R.A., 2003. Sparse finite elements for elliptic problems with stochastic loading. Numerische Mathematik 95 (4), 707–734.
Simiu, E., Scanlan, R., 1996. Wind Effects on Structures: Fundamentals and Applications to Design. Wiley, New York.
Sun, Q., Boyd, I.D., 2004. Flat-plate aerodynamics at very low Reynolds number. Journal of Fluid Mechanics 502, 199–206.
Sunada, S., Sakaguchi, A., Kawachi, K., 1997. Airfoil section characteristics at a low Reynolds number. Journal of Fluids Engineering 119, 129–135.
Troen, I., Petersen, E., 1989. European Wind Atlas. Risø National Laboratory, Roskilde, Denmark.
Wan, X., Karniadakis, G.E., 2006a. Long-term behavior of polynomial chaos in stochastic flow simulations. Computer Methods in Applied Mechanics and Engineering 195, 5582–5596.
Wan, X., Karniadakis, G.E., 2006b. Multi-element generalized polynomial chaos for arbitrary probability measures. SIAM Journal on Scientific Computing 28 (3), 901–928 (electronic).
Wiener, N., 1938. The homogeneous chaos. American Journal of Mathematics 60, 897–936.
Xiu, D., Karniadakis, G.E., 2002. The Wiener–Askey polynomial chaos for stochastic differential equations. SIAM Journal on Scientific Computing 24 (2), 619–644 (electronic).
Xiu, D., Karniadakis, G.E., 2003. Modeling uncertainty in flow simulations via generalized polynomial chaos. Journal of Computational Physics 187 (1), 137–167.